Title

Visible Light-Responsive DASA-Polymer Conjugates.

Journal

ACS macro letters, 6(7)

ISSN

2161-1653

Authors

Ulrich, Sebastian

Hemmer, James R

Page, Zachariah A

et al.

Publication Date

2017-07-01

DOI

10.1021/acsmacrolett.7b00350

Peer reviewed

ACS Macro Letters

Letter

pubs.acs.org/macroletters

Visible Light-Responsive DASA-Polymer Conjugates

Sebastian Ulrich,[†,‡,§] James R. Hemmer,[†,∥] Zachariah A. Page,[⊥] Neil D. Dolinski,[⊥] Omar Rifaie-Graham,[§] Nico Bruns,[§] Craig J. Hawker,[∥,⊥] Luciano F. Boesel,[*,‡] and Javier Read de Alaniz[*,∥]

[‡]Empa, Swiss Federal Laboratories for Materials Science and Technology, Laboratory for Biomimetic Membranes and Textiles, Lerchenfeldstrasse 5, 9014 St. Gallen, Switzerland

[∥]Department of Chemistry and Biochemistry and [⊥]Materials Department, Materials Research Laboratory, University of California, Santa Barbara, California 93106, United States

[§]Adolphe Merkle Institute, University of Fribourg, Chemin des Verdiers 4, 1700 Fribourg, Switzerland

Supporting Information

ABSTRACT: A modular synthesis of Donor–Acceptor Stenhouse Adduct (DASA) polymer conjugates is described. Pentafluorophenyl-ester chemistry is employed to incorporate aromatic amines into acrylate and methacrylate copolymers, which are subsequently coupled with activated furans to generate polymers bearing a range of DASA units in a modular manner. The effect of polymer glass transition temperature on switching kinetics is studied, showing dramatic rate enhancements in going from a glassy to a rubbery matrix. Moreover, tuning the DASA absorption profile allows for selective switching, as demonstrated by ternary photopatterning, with potential applications in rewriteable data storage.

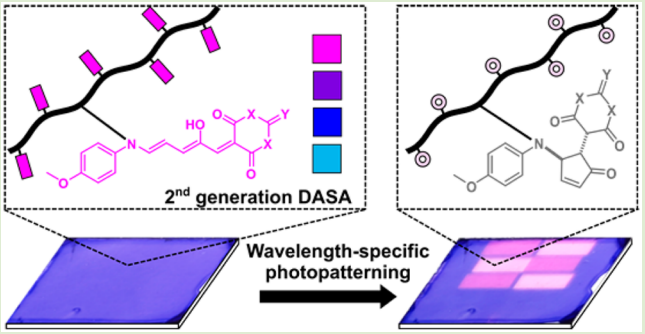

Organic photoswitches that rapidly alter their properties upon irradiation have been a subject of intense research for stimuli-responsive materials platforms. Light as a stimulus offers unique advantages, including excellent spatial and temporal precision, along with selective activation[1] to control material properties. Photoswitches have been incorporated within polymer scaffolds, nanoparticles, and biomolecules, with applications ranging from actuators to sensors to drug delivery.[2−6] However, traditional photoswitches require the use of high-energy ultraviolet (UV) light, which has limited their development and utility, especially with regard to biomedical applications where the UV light presents a skin hazard, causes fatigue, and limits penetration depth. To overcome these limitations, a novel class of visible light-responsive negative photoswitches, termed donor–acceptor Stenhouse adducts (DASAs), were recently developed.[7−10] The first generation DASAs, possessing dialkylamino donors, have been employed in a number of applications, ranging from sensing to drug delivery.[11−18] However, transitioning to aromatic amine-based donors provides second generation DASA derivatives, allowing for tunable absorption (450−750 nm) and improved switchability in a variety of solvents.[19,20] To fully exploit these new properties in visible light-responsive materials it became apparent that a synthetic strategy to conjugate DASAs to polymers needed to be developed. Herein we describe a modular approach using activated ester chemistry.

Both pentafluorophenyl acrylate (**PFPA**) and methacrylate (**PFPMA**) have found widespread use in polymer conjugation due to their high selectivity/reactivity toward primary amines.[21−23] Their successful application in a variety of polymeric systems, ranging from polymer brushes and layer-by-layer assemblies to nanogels, demonstrates their versatility as a synthetic platform.[24−28] In exploiting this chemistry and postpolymerization functionalization strategies, aromatic amine precursors were installed and subsequently reacted with activated furans to incorporate the corresponding DASA adducts. Given the modular nature of this approach, a variety of DASA–polymer conjugates with tunable color were synthesized and structure–property relationships ascertained. In particular, the ability to tune switching kinetics based on polymer glass transition temperature (T_g) and ability to selectively photopattern uniform thin films based on tunable DASA absorption profile is demonstrated.

The general synthetic strategy to DASA–polymer conjugates is provided in Figure 1a. First, copolymers containing **PFP(M)A** were reacted with an excess of aromatic amine precursors bearing reactive primary amines as the linking site. Notably, milder reaction conditions were required for acrylate- relative to methacrylate-based polymers, which is attributed to enhanced reactivity of **PFPA** over **PFPMA**.[21] In a second step, the aniline-modified polymer backbones were reacted with an excess of activated furan to yield pendant DASAs. A set of two aromatic amine precursors, *N*-(4-methoxyphenyl)-1,3-diamino-

Received: May 10, 2017
Accepted: June 13, 2017
Published: June 23, 2017

DOI: 10.1021/acsmacrolett.7b00350
ACS Macro Lett. 2017, 6, 738−742

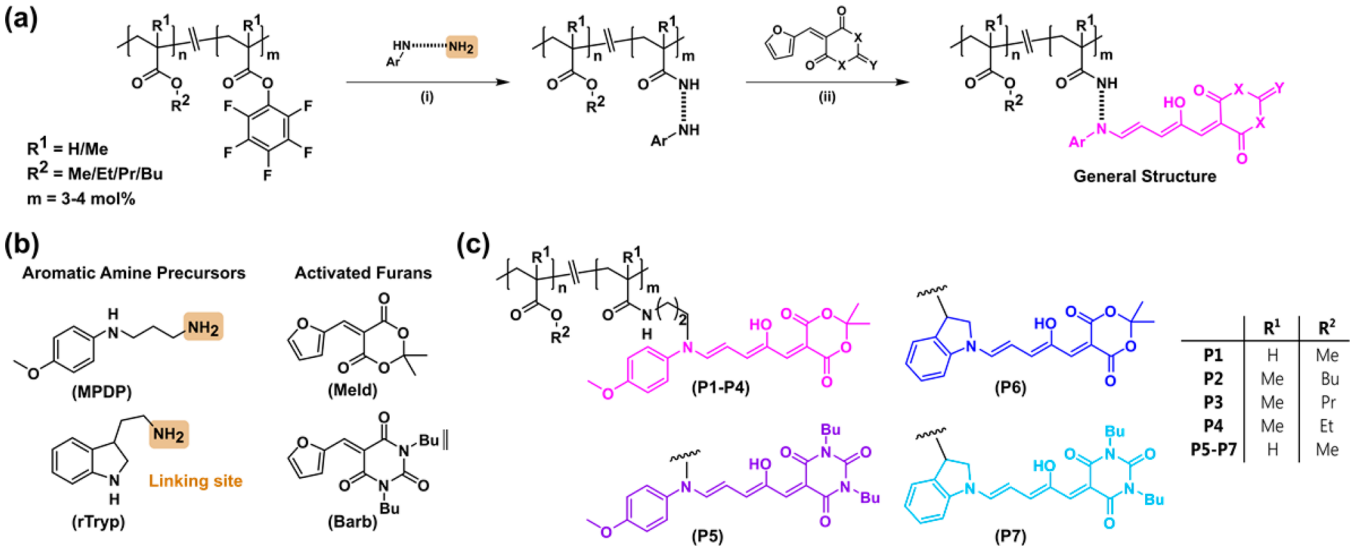

Figure 1. DASA–polymer conjugate platform. (a) General synthesis of DASA–polymer conjugates. Reagents and conditions: (i) aniline precursor/TEA and THF/40 °C/1–2 days for acrylate and DMF/50 °C/2–3 days for methacrylate copolymers, (ii) furan adduct/THF/rt/several days. (b) Structures of aromatic amine precursors and activated furans. (c) Structures of all synthesized DASA–polymer conjugates **P1**–**P7**.

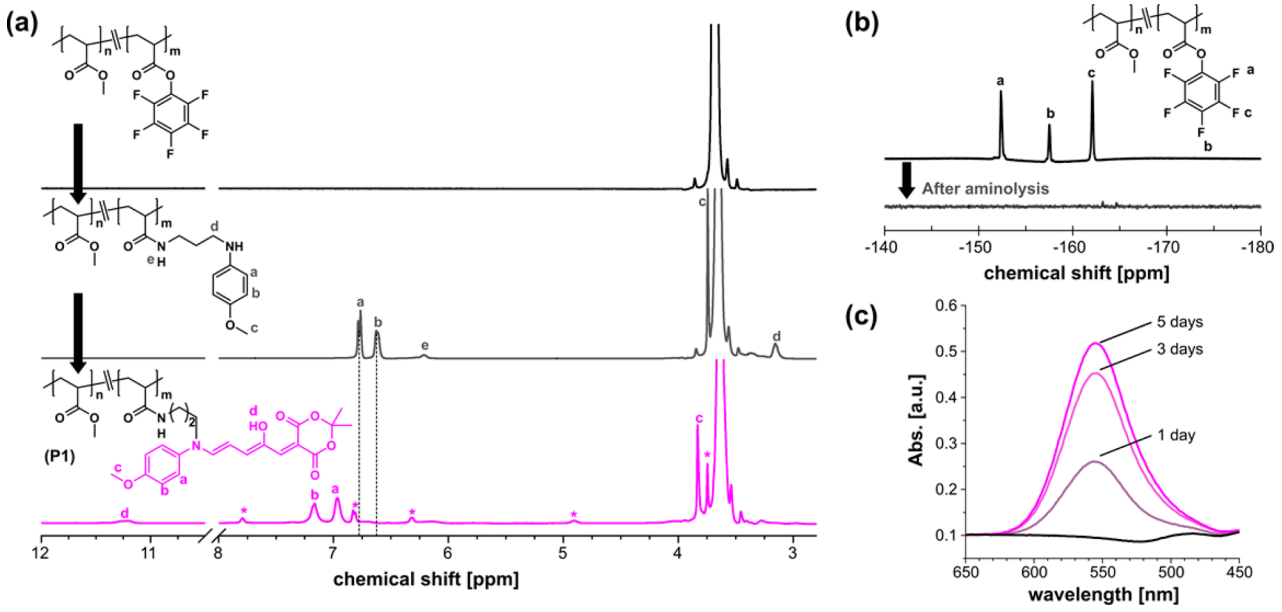

Figure 2. Synthesis monitoring and characterization of DASA–polymer conjugate **P1**. (a) Diffusion-edited ^{1}H NMR of synthetic steps to **P1** (closed state DASA signals indicated by an asterisk). Vertical lines illustrate the disappearance of aromatic amine signals. (b) ^{19}F NMR tracking of active ester aminolysis. (c) UV–vis absorption spectroscopic tracking of DASA formation.

propane (**MPDP**) and 2-(indolin-3-yl)ethan-1-amine (**rTryp**), and two activated furans based on Meldrum's acid (**Meld**) and Barbituric acid (**Barb**) were employed (Figure 1b). Taking advantage of this modular protocol led to the generation of a library of DASA–polymer conjugates (Figure 1c). First, polymers bearing pendent **MPDP-Meld** DASAs (~4 mol %) were synthesized, altering the matrix from poly(methyl acrylate) (**PMA**) to poly(butyl methacrylate) (**PBMA**), poly(propyl methacrylate) (**PPMA**), and poly(ethyl methacrylate) (**PEMA**), which corresponds to copolymers **P2**, **P3**, and **P4**, respectively. While the DASA architecture is the same for **P1**–**P4**, the T_g values for the parent polymer vary by ~55 °C, with literature reports of 9, 20, 35, and 65 °C for **PMA**, **PBMA**, **PPMA**, and **PEMA**.[29] Differential scanning calorimetry (DSC) of the DASA–polymer conjugates indicated an increase of T_g by ~14 °C relative to the parent polymers, which was accounted for during all measurements (Table S3). To provide access to material with a tunable absorption profile while maintaining a similar T_g, DASAs from all possible combinations of aromatic amine precursors (donor group) and activated furans (acceptor group) were incorporated into **PMA** copolymers. Specifically, this yielded **MPDP-Barb**, **rTryp-Meld**, and **rTryp-Barb** derivatives, corresponding to **P5**, **P6**, and **P7**, respectively.

Conveniently, the syntheses could be tracked using a combination of ^{19}F and ^{1}H NMR spectroscopies (Figure 2) with further characterization by diffusion-edited ^{1}H NMR, ultraviolet–visible (UV–vis) absorption, and Fourier transform infrared spectroscopy (FT-IR; Figures 2 and S1–7). For example, ^{19}F NMR spectroscopy with pentafluorophenol as an

DOI: 10.1021/acsmacrolett.7b00350
ACS Macro Lett. 2017, 6, 738–742

internal standard reveals the incorporation of **PFPA** (~3 mol %) in a copolymer of poly(methyl acrylate-*co*-**PFPA**) P(MA-*co*-**PFPA**) (Figure S1). Reaction of this copolymer with **MPDP** results in the clean appearance of anisidine proton signals at 6.75 and 6.60 ppm with ^{1}H NMR monitoring, suggesting high selectivity of the primary amine over the aromatic secondary amine (Figure 2a). Significantly, the complementary loss in fluorine signal with ^{19}F NMR monitoring reveals quantitative conversion (Figure 2b). Subsequently, reaction with an excess of **Meld** yields the DASA–polymer conjugate **P1** after ~5 days. DASA formation was monitored over time with UV–vis spectroscopy, where a diminishing change in absorbance was used to indicate reaction completion (Figure 2c, see SI for more details). Complete DASA formation was confirmed by ^{1}H NMR with the disappearance of the anisidine signals and the appearance of the DASA signals of the open and the equilibrium closed state being diagnostic (marked by asterisk). Preparative size exclusion chromatography (SEC) was utilized as an efficient means to purify **P1**, and subsequent DASA–polymer conjugates with the strong dye character of the DASA–polymer conjugates allowing this process to be conveniently monitored by eye.

A key advantage of second generation DASA is their color tunability over a wide range.[19] To investigate the absorption profile of the DASA–polymer conjugates, uniform thin films were spin coated from solution for all DASA derivatives (**P1**, **P5**–**P7**) with their UV–vis absorption spectra being shown in Figure 3a. Impressively, the solid-state absorption maximum was shifted from 554 to 620 nm, when comparing **P1** to **P7**, which is related to the relative donor and acceptor strength. To qualitatively study their photochromic behavior, the thin films were then irradiated with white light, resulting in discoloration, which could be reversed upon heating (Figure 3b). This reversible photoswitching highlights the improved properties of second generation DASAs compared to the first generation, for which only irreversible decoloration was observed in thin films (Figure S22). The ability to generate several DASA–polymer conjugates with reversible photochromism from one PFP-copolymer highlights the versatility and modularity of the presented approach.

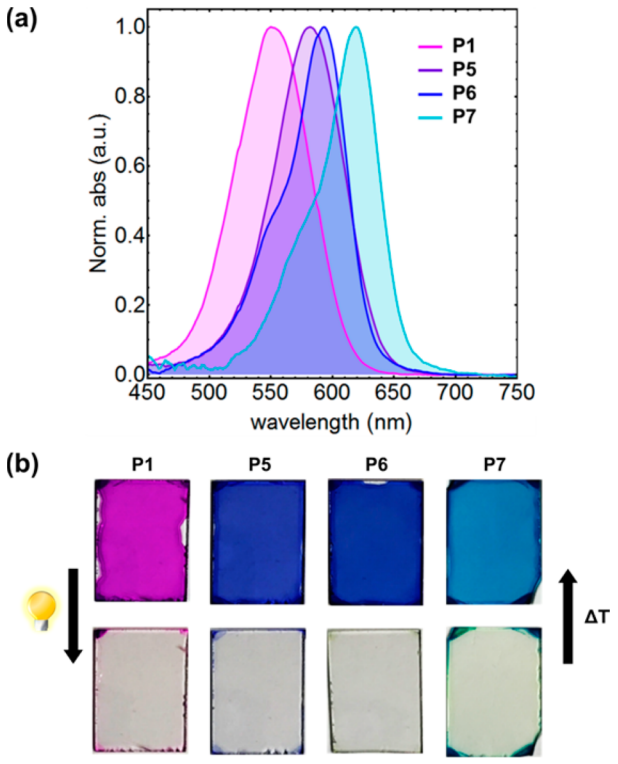

Figure 3. Spin-coated uniform thin films of DASA–polymer conjugates **P1** and **P5**–**P7**. (a) Normalized thin film UV–vis absorption profiles. (b) Photographic images of thin films before and after white light illumination or thermal equilibration, respectively (for details, see Supporting Information).

To study the effect of the surrounding matrix on switching kinetics, the four **MPDP-Meld** based polymers (**P1**–**P4**) were compared as uniform thin films on glass (Figure 4). First, the thin films were brought above their parent T_g and irradiated with white light to photoswitch all DASAs to the colorless closed state. The samples were then cooled down to 40 °C and the thermal isomerization at 40 °C to the colored state was monitored with absorption spectroscopy (Figure 4b). After reaching equilibrium at 40 °C, indicated by an absorption plateau, the samples were annealed above T_g, cooled back to 40 °C, and remeasured. This post-treatment allowed for equilibration in a viscous state and the measured absorption was normalized to 1 in Figure 4b. Interestingly, **P1** and **P2** equilibrated in a few hours, while **P3** and **P4** required >24 h to reach equilibrium. Moreover, postannealing revealed no change in absorption for **P1** and **P2** (parent T_g < 40 °C), while **P3** (parent T_g near 40 °C) and **P4** (parent T_g > 40 °C) each showed a large increase in absorption. This suggests that thermal isomerization of the pendent DASAs from the colorless state to the colored state is impeded within a glassy matrix. Moreover, due to the large increase in molecular volume that accompanies thermal equilibration of DASAs, the molecules may be "trapped" at a lower colored/colorless ratio compared to above T_g, as seen in Figure 4b. This dramatic effect of T_g on switching kinetics was also observed by monitoring the change in absorbance of **P3** at 20 °C, which is below the parent T_g (35 °C), followed by ramping the temperature to 65 °C (Figure 4c). Impressively, little-to-no change in absorbance was noted below T_g over ~68 h, while heating led to comparatively rapid isomerization to equilibrium. These effects were also noted for photoisomerization ("switching") kinetics (a.k.a., samples under irradiation), as shown in Figure 4d. **P4** (parent T_g = 65 °C) and **P2** (parent T_g = 20 °C) were irradiated while at 40 °C, causing rapid switching of **P4**, but not **P2**. The distinct effect of T_g on switching kinetics provides a tunable handle for DASA–polymer conjugates, which will aid in the development of next generation smart materials.

Varying DASA absorption provides an alternative tunable handle that allows for selective switching. As demonstrated earlier, modifying the donor and acceptor components provided **P1** and **P7**, which have little absorption overlap at ~620 nm. Blending the two copolymers and casting a uniform thin film leads to a linear combination of absorption profiles, as shown in Figure 5a, suggesting a lack of ground state charge transfer. Significantly, irradiating the film with orange light (λ_{max} = 617 nm) gives rise to a rapid decrease in absorption for the low energy peak that corresponds to **P7**, leaving behind **P1** DASA in its colored state (Figure 5a). This has potential applications in rewriteable data storage that extends beyond binary coding given the system's reversible switchability and selectivity.[30] As a demonstration, the blended polymer film was irradiated through a photomask with white light, switching both DASA components to their colorless state (Figure 5b).

DOI: 10.1021/acsmacrolett.7b00350
ACS Macro Lett. 2017, 6, 738–742

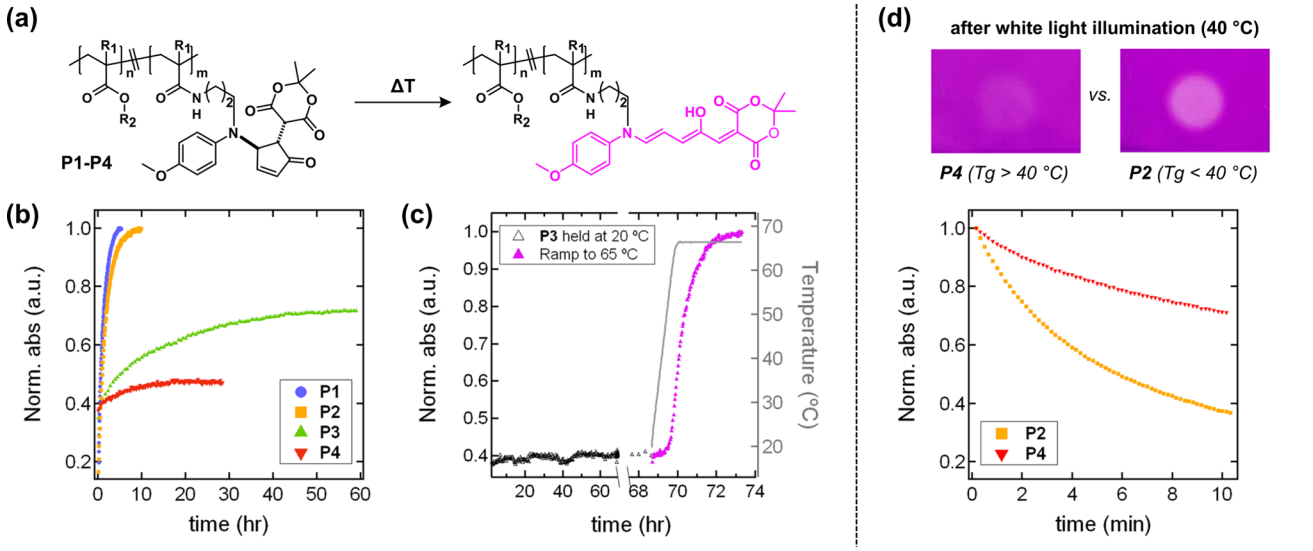

Figure 4. Effect of T_g on switching kinetics in thin films. (a) Chemical structures for **P1**−**P4** in going from a colorless to a colored state. (b) Thermal equilibration of **P1**−**P4** at 40 °C, showing faster equilibration for **P1** and **P2**, which are above the T_g of the parent polymer matrix, compared to **P3** and **P4**, which are near and below T_g of the parent polymer matrix, respectively. The absorbance is normalized to that obtained after annealing above T_g, showing that **P3** and **P4** get "trapped" in a glassy matrix. (c) Transitioning from a glassy to a more viscous state for **P3** using a temperature ramp from 20 to 65 °C, providing a fast increase in absorption upon heating. (d) Photoswitching **P2** and **P4** with white light at 40 °C and corresponding kinetics.

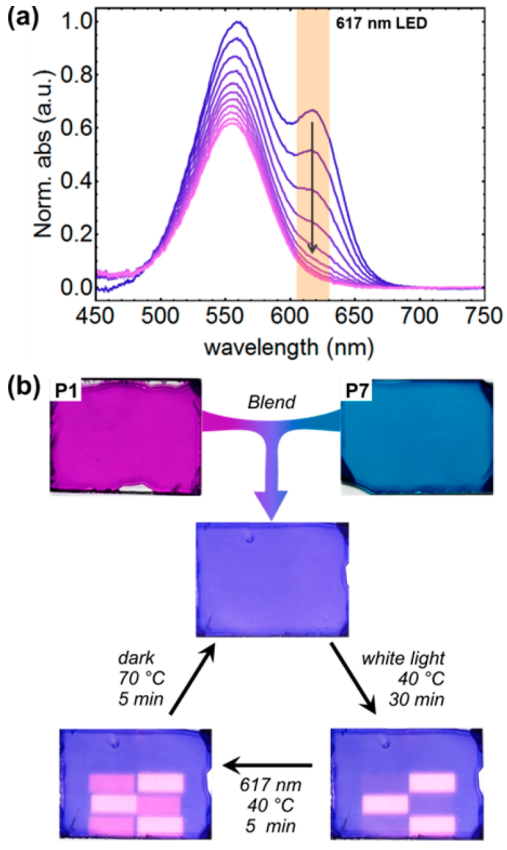

Figure 5. Selective switching of DASA−polymer conjugates in thin film blends of **P1** and **P7**. (a) Photoswitching kinetics upon irradiation with an orange LED. (b) Digital images of **P1**, **P7**, and **P1**+**P7** thin films, and photopatterning of the blended film to generate a ternary pattern. Sample dimensions are 15 × 20 mm^2.

Subsequent irradiation with orange light through an alternate photomask selectively switches **P7**, providing a ternary pattern containing three states: both colored, purple; both bleached, colorless; and **P1** colored/**P7** colorless, pink. The pattern can then be completely erased through heating the sample above T_g, returning the film to the full colored state.[31,32] This efficient pattern transfer is made possible by covalently binding the DASAs to polymers, since it eliminated phase separation and allows for the facile fabrication of uniform films. Furthermore, fine patterns with structural features below 100 μm could be achieved (Figure S23).

In summary, second generation DASA−polymer conjugates were synthesized by taking advantage of selective PFP-ester chemistry. NMR, FTIR, and UV−vis analyses demonstrate quantitative postpolymerization functionalization for the incorporation of aromatic amine derivatives, followed by ring-opening to form a library of DASA derivatives. The modular platform provides access to polymer matrices with varied T_g and pendent DASAs with tunable absorption, both of which act as handles to alter switching kinetics. The demonstrated selectivity will guide and encourage the development of next generation smart materials in areas such as sensing and data storage.

■ ASSOCIATED CONTENT

Supporting Information

The Supporting Information is available free of charge on the ACS Publications website at DOI: 10.1021/acsmacrolett.7b00350.

Experimental conditions and supplementary data (PDF).

■ AUTHOR INFORMATION

Corresponding Authors

*E-mail: luciano.boesel@empa.ch.

*E-mail: javier@chem.ucsb.edu.

ORCID

Nico Bruns: 0000-0001-6199-9995

Craig J. Hawker: 0000-0001-9951-851X

DOI: 10.1021/acsmacrolett.7b00350
ACS Macro Lett. 2017, 6, 738−742

Javier Read de Alaniz: 0000-0003-2770-9477

Author Contributions

†These authors contributed equally to this work.

Notes

The authors declare no competing financial interest.

■ ACKNOWLEDGMENTS

We thank the National Science Foundation (MRSEC program, DMR 1121053) and California NanoSystem Institute (CNSI) Challenge Grant Program for support. The Swiss National Science Foundation (SNSF) is acknowledged for the partial financial support to LFB through Grant No. 200021_172609 ("Teleflow"), to the partial financial support to the NMR hardware through Grant No. 150638, and to financial support to N.B. through Grant No. PP00P2_144697 and the NCCR Bio-Inspired Materials. We thank Dr. Alexander Mikhailovsky for his help constructing the optical setup used for the cycling and selective switching experiments. We thank Dr. Daniel Rentsch (Empa) for NMR measurements and support.

■ REFERENCES

(1) Lerch, M. M.; Hansen, M. J.; Velema, W. A.; Szymanski, W.; Feringa, B. L. *Nat. Commun.* **2016**, *7*, 12054.
(2) Pauly, A. C.; Schöller, K.; Baumann, L.; Rossi, R. M.; Dustmann, K.; Ziener, U.; Courten, D. d.; Wolf, M.; Boesel, L. F.; Scherer, L. *Sci. Technol. Adv. Mater.* **2015**, *16* (3), 034604.
(3) Schöller, K.; Küpfer, S.; Baumann, L.; Hoyer, P. M.; de Courten, D.; Rossi, R. M.; Vetushka, A.; Wolf, M.; Bruns, N.; Scherer, L. J. *Adv. Funct. Mater.* **2014**, *24* (33), 5194−5201.
(4) Klajn, R. *Chem. Soc. Rev.* **2014**, *43* (1), 148−184.
(5) Klajn, R.; Stoddart, J. F.; Grzybowski, B. A. *Chem. Soc. Rev.* **2010**, *39* (6), 2203−2237.
(6) Zhang, J. J.; Zou, Q.; Tian, H. *Adv. Mater.* **2013**, *25* (3), 378−399.
(7) Helmy, S.; Leibfarth, F. A.; Oh, S.; Poelma, J. E.; Hawker, C. J.; Read de Alaniz, J. *J. Am. Chem. Soc.* **2014**, *136* (23), 8169−8172.
(8) Helmy, S.; Oh, S.; Leibfarth, F. A.; Hawker, C. J.; Read de Alaniz, J. *J. Org. Chem.* **2014**, *79* (23), 11316−11329.
(9) Laurent, A. D.; Medved, M.; Jacquemin, D. *ChemPhysChem* **2016**, *17* (12), 1846−1851.
(10) Lerch, M. M.; Wezenberg, S. J.; Szymanski, W.; Feringa, B. L. *J. Am. Chem. Soc.* **2016**, *138* (20), 6344−6347.
(11) Mason, B. P.; Whittaker, M.; Hemmer, J.; Arora, S.; Harper, A.; Alnemrat, S.; McEachen, A.; Helmy, S.; Read de Alaniz, J.; Hooper, J. P. *Appl. Phys. Lett.* **2016**, *108* (4), 041906.
(12) Diaz, Y. J.; Page, Z. A.; Knight, A. S.; Treat, N. J.; Hemmer, J. R.; Hawker, C. J.; Read de Alaniz, J. *Chem. - Eur. J.* **2017**, *23*, 3562−3566.
(13) Singh, S.; Friedel, K.; Himmerlich, M.; Lei, Y.; Schlingloff, G.; Schober, A. *ACS Macro Lett.* **2015**, *4* (11), 1273−1277.
(14) Balamurugan, A.; Lee, H.-i. *Macromolecules* **2016**, *49*, 2568−2574.
(15) Poelma, S. O.; Oh, S. S.; Helmy, S.; Knight, A. S.; Burnett, G. L.; Soh, H. T.; Hawker, C. J.; Read de Alaniz, J. *Chem. Commun.* **2016**, *52* (69), 10525−10528.
(16) Sinawang, G.; Wu, B.; Wang, J.; Li, S.; He, Y. *Macromol. Chem. Phys.* **2016**, *217* (21), 2409−2414.
(17) Dolinski, N. D.; Page, Z. A.; Eisenreich, F.; Niu, J.; Hecht, S.; Read de Alaniz, J.; Hawker, C. J. *ChemPhotoChem.* **2017**, *1*, 125−131.
(18) Jia, S.; Du, J. D.; Hawley, A.; Fong, W.-K.; Graham, B.; Boyd, B. J. *Langmuir* **2017**, *33*, 2215−2221.
(19) Hemmer, J. R.; Poelma, S. O.; Treat, N.; Page, Z. A.; Dolinski, N. D.; Diaz, Y. J.; Tomlinson, W.; Clark, K. D.; Hooper, J. P.; Hawker, C.; Read de Alaniz, J. *J. Am. Chem. Soc.* **2016**, *138* (42), 13960−13966.
(20) Mallo, N.; Brown, P. T.; Iranmanesh, H.; MacDonald, T. S. C.; Teusner, M. J.; Harper, J. B.; Ball, G. E.; Beves, J. E. *Chem. Commun.* **2016**, *52* (93), 13576−13579.
(21) Eberhardt, M.; Mruk, R.; Zentel, R.; Théato, P. *Eur. Polym. J.* **2005**, *41* (7), 1569−1575.
(22) Mohr, N.; Barz, M.; Forst, R.; Zentel, R. *Macromol. Rapid Commun.* **2014**, *35* (17), 1522−1527.
(23) Das, A.; Theato, P. *Chem. Rev.* **2016**, *116* (3), 1434−1495.
(24) Kessler, D.; Jochum, F. D.; Choi, J.; Char, K.; Theato, P. *ACS Appl. Mater. Interfaces* **2011**, *3* (2), 124−128.
(25) Choi, J.; Schattling, P.; Jochum, F. D.; Pyun, J.; Char, K.; Theato, P. *J. Polym. Sci., Part A: Polym. Chem.* **2012**, *50* (19), 4010−4018.
(26) Nuhn, L.; Tomcin, S.; Miyata, K.; Mailander, V.; Landfester, K.; Kataoka, K.; Zentel, R. *Biomacromolecules* **2014**, *15* (11), 4111−4121.
(27) Scherer, M.; Kappel, C.; Mohr, N.; Fischer, K.; Heller, P.; Forst, R.; Depoix, F.; Bros, M.; Zentel, R. *Biomacromolecules* **2016**, *17*, 3305−3317.
(28) Seo, J.; Schattling, P.; Lang, T.; Jochum, F.; Nilles, K.; Theato, P.; Char, K. *Langmuir* **2010**, *26* (3), 1830−1836.
(29) Wood, L. A. *J. Polym. Sci.* **1958**, *28* (117), 319−330.
(30) Wei, P.; Li, B.; de Leon, A.; Pentzer, E. *J. Mater. Chem. C* **2017**, n/a.
(31) Wu, N. M.-W.; Wong, H.-L.; Yam, V. W.-W. *Chem. Sci.* **2017**, *8* (2), 1309−1315.
(32) Garai, B.; Mallick, A.; Banerjee, R. *Chem. Sci.* **2016**, *7* (3), 2195−2200.

DOI: 10.1021/acsmacrolett.7b00350
ACS Macro Lett. 2017, 6, 738−742